0.4 THz Photonic-Wireless Link With 106 Gb/s Single Channel Bitrate

Jia, Shi; Pang, Xiaodan; Ozolins, Oskars; Yu, Xianbin; Hu, Hao; Yu, Jinlong; Guan, Pengyu; Da Ros, Francesco; Popov, Sergei; Jacobsen, Gunnar

Total number of authors:
14

Published in:
Journal of Lightwave Technology

Link to article, DOI:
10.1109/JLT.2017.2776320

Publication date:
2018

Document Version
Peer reviewed version

This project has received Funding from the European Union's Seventh Framework Programme and Horizon 2020 Research and Innovation Programme under Marie Sklodowska-Curie Actions grant no. 713683 (H2020)

0.4 THz Photonic-Wireless Link with 106 Gbit/s Single Channel Bitrate

Shi Jia, Xiaodan Pang, *Member, IEEE*, Oskars Ozolins, *Member, IEEE*, Xianbin Yu, *Senior Member, IEEE*, Hao Hu, Jinlong Yu, Pengyu Guan, Francesco Da Ros, Sergei Popov, Gunnar Jacobsen, Michael Galili, Toshio Morioka, *Fellow, OSA,* Darko Zibar, and Leif K. Oxenløwe
(*Invited Paper*)

***Abstract*—To accommodate the demand of exponentially increased global wireless data traffic, the prospective data rates for wireless communication in the market place will soon reach 100 Gbit/s and beyond. In the lab environment, wireless transmission throughput has been elevated to the level of over 100 Gbit/s attributed to the development of photonic-assisted millimeter wave (MMW) and THz technologies. However, most of recent demonstrations with over 100 Gbit/s data rates are based on spatial or frequency division multiplexing techniques, resulting in increased system's complexity and energy consumption. Here, we experimentally demonstrate a single channel 0.4 THz photonic-wireless link achieving a net data rate of beyond 100 Gbit/s by using a single pair of THz emitter and receiver, without employing any spatial/frequency division multiplexing techniques. The high throughput up to 106 Gbit/s within a single THz channel is enabled by combining spectrally efficient modulation format, ultra-broadband THz transceiver and advanced digital signal processing (DSP) routine. Besides that, our demonstration from system-wide implementation viewpoint also features high transmission stability, and hence shows its great potential to not only decrease the system's complexity, but also meet the requirements of prospective data rates for bandwidth-hungry short-range wireless applications.**

***Index Terms*—Radio frequency photonics, single channel, THz wireless transmission, ultrafast information processing**

This work was supported in part by China Postdoctoral Science Foundation under Grant 2017M611990, in part by Danish center of excellence CoE SPOC under Grant DNRF123, in part by European Research Council ERC-PoC project TWIST under Grant 641420, and in part by Natural National Science Foundation of China (NSFC) under Grant 61427817 and 61405142.

S. Jia and X. Yu are with the College of Information Science and Electronic Engineering, Zhejiang University, Hangzhou 310027, China, and S. Jia was also with the DTU Fotonik, Department of Photonics Engineering, Technical University of Denmark, DK-2800, Kgs. Lyngby, Denmark. (xyu@zju.edu.cn, jiashizju@zju.edu.cn).

X. Pang is with the School of ICT, KTH Royal Institute of Technology, Electrum 229, Kista, SE-164 40, Sweden. X. Pang, O. Ozolins, and G. Jacobsen are with the NETLAB, RISE Acreo AB, SE-16425 Kista, Sweden. S. Popov is with the School of SCI, KTH Royal Institute of Technology, Electrum 229, Kista, SE-164 40, Sweden. (xiaodan@kth.se).

H. Hu, P. Guan, F. D. Ros, M. Galili, T. Morioka, D. Zibar, and L. K. Oxenløwe are with the DTU Fotonik, Department of Photonics Engineering, Technical University of Denmark, DK-2800, Kgs. Lyngby, Denmark. (lkox@fotonik.dtu.dk).

J. Yu is with the School of Electronic Information Engineering, Tianjin University, Tianjin 300072, China.

I. Introduction

With the coming of Big Data Era (BDE) and Internet of Things (IoT) targeting the interconnection of everything, the global net data traffic is increasing exponentially [1], [2]. The ultrafast wireless network (UWN), as the supporter for carrying the fastest-growing part, is foreseeable to play a key role in the future internet [3]. Historically, from the comparison of the 3rd-generation (3G)/4G and upcoming global 5G networks, carrier frequencies used for wireless communications have been increasing step by step [4]-[7], to meet bandwidth requirements for delivering higher net data rates. In this context, the speed of wireless transmissions has been demonstrated in the laboratories to a new level of beyond 100 Gbit/s, by the rapid development of photonic-assisted millimeter wave (MMW) and terahertz (THz, >300 GHz) technologies [8], [9]. Such an ultrafast data rate will be the prospective for wireless communication in the market place within 10 years [10].

The full exploitation of ultra-broad bandwidth at high carrier frequencies of over 60 GHz, and the utilization of spectrally efficient modulation formats and advanced multiplexing techniques are the main driving factors to enable the realization of beyond 100 Gbit/s net date rate [8]. In recent years, a few experimental demonstrations of wireless transmissions at 100 Gbit/s and beyond, have been reported, operating in different frequency bands ranging from MMW to THz. In the W-band (75-110 GHz), demonstrations with data rates of from 100 Gbit/s to 400 Gbit/s have been achieved by using the techniques incorporating optical polarization division multiplexing (PDM) and wireless spatial multiple-input multiple-output (MIMO) [11]-[14]. In the D-band (110-170 GHz), a 100 Gbit/s and a 352 Gbit/s wireless transmissions have been reported incorporating frequency division multiplexing (FDM), PDM and spatial MIMO techniques [15][16]. In the sub-THz band (200-300 GHz), spatial single-input single-output (SISO) wireless communication systems in the order of 100 Gbit/s have been demonstrated by employing frequency division multiplexing techniques based on optical frequency comb (OFC) sources [17]-[21]. To move beyond this, the THz band (300 GHz-10 THz) featuring an extremely large bandwidth available between the millimeter-wave and infrared radiation is considered as the "Next Frontier" to meet the data rate target of future UWNs.

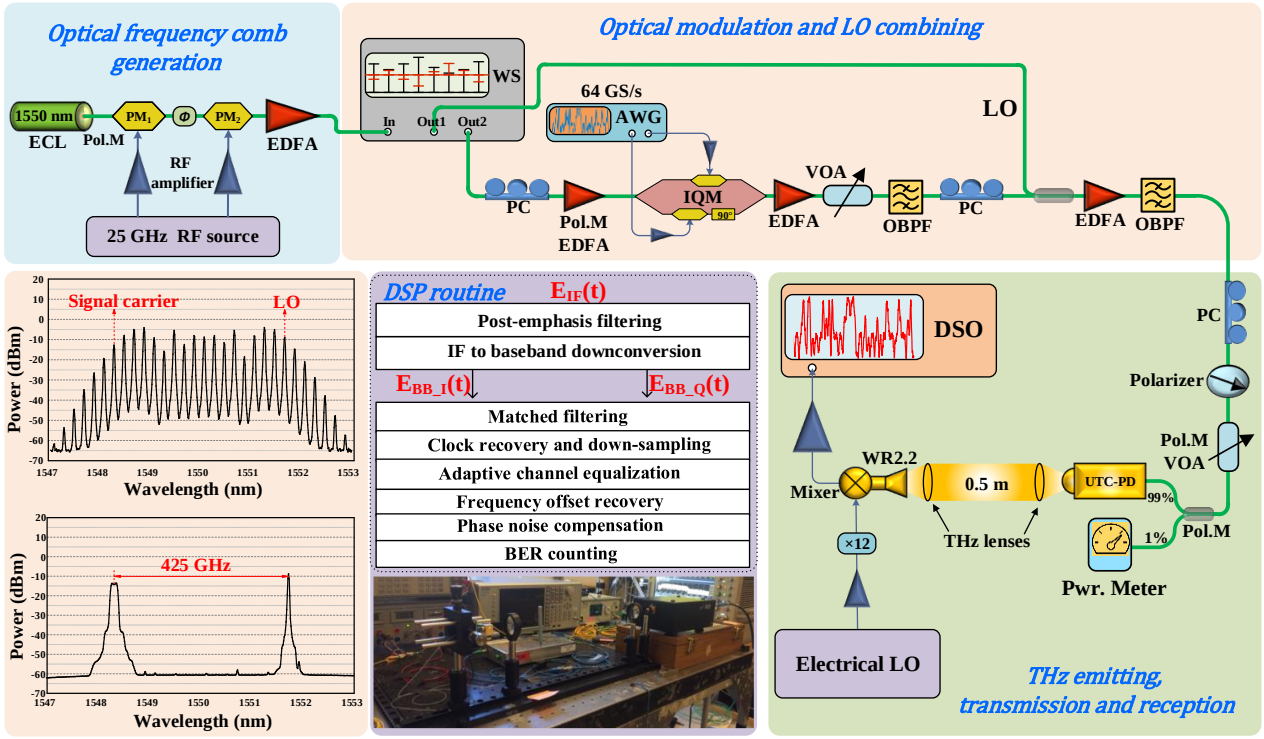

Fig. 1. Experimental setup of the single channel photonic-wireless link in the 0.4 THz band. ECL: external cavity laser, Pol. M: polarization maintaining, PM: phase modulator, RF: radio frequency, EDFA: Erbium doped fiber amplifier, WS: wave shaper, AWG: arbitrary waveform generator, IQM: in-phase and quadrature modulator, VOA: variable optical attenuator, OBPF: optical band-pass filter, PC: polarization controller, LO: local oscillator, UTC-PD: uni-travelling carrier photodiode, DSO: digital sampling oscilloscope. Insets: optical spectra of the generated optical frequency comb (up-left) and combined modulated signal and LO (down-left), and the DSP routine structure at the receiver (up-middle) and a picture of the actual setup (down-middle).

In the THz band, we have recently contributed to the development of THz wireless communication by demonstrating a series of high-speed photonic wireless transmission systems in the 0.3-0.5 THz regime with multi-channel Nyquist-quadrature phase shift keying (QPSK)/16 quadrature amplitude modulation (QAM) signals, [22]-[31]. These work is enabled by ultrafast THz transceivers, particularly the availability of ultra-broadband uni-travelling photodiodes (UTC-PDs) as efficient photo-mixing emitters and Schottky diodes as broadband electronic receivers, and the highest net data rate has reached up to 260 Gbit/s [31]. However, most of the demonstrations aforementioned are in view of the optical PDM, and/or the spatial MIMO and/or the frequency multiplexing techniques, all of which will in turn increase the system's size, energy consumption and the complexity in terms of both the hardware and the digital signal processing (DSP) module, resulting in increased overall cost. Therefore, a single channel wireless transmission system at a data rate of over 100 Gbit/s without employing multiplexing techniques, will show an exciting potential to not only low down the system's energy consumption, complexity and cost, but also meet the requirements of prospective data rates for future UWNs and burgeon bandwidth-hungry wireless applications.

In this paper, we propose and experimentally demonstrate a single channel THz photonic-wireless transmission system at the 0.4 THz band without using any multiplexing techniques, reaching a net data rate of up to over 100 Gbit/s based on a single pair of THz emitter and receiver. The capacity of over 100 Gbit/s within a single channel is enabled by combining 16QAM modulation format, ultra-broadband THz transceivers and a tailored DSP routine with pre- and post-equalization, which can accurately reconstruct the frequency response within a single broadband THz channel. At the transmitter side, an OFC source is coherently generated for photonic heterodyne mixing in an ultra-wideband antenna integrated UTC-PD [32], which generates and radiates a single channel THz signal with high frequency stability. At the reception side, the over 100 Gbit/s wirelessly propagated 400 GHz band signal is received in a Schottky mixer based electrical receiver. Finally, we have successfully recovered up to 32 Gbaud wirelessly transmitted 16QAM signals in the experiment, resulting in pre-forward error correction (FEC) line rates of up to 128 Gbit/s and post-FEC error-free bit rates of up to 106 Gbit/s in a single THz channel.

To extend the operational principle and details of the experiment, as well as the DSP routine based on our previous work reported in [33], this paper is organized as follows. In Section II, we present the details of our THz photonic-wireless link with an emphasis on the experimental setup and DSP routine. Section III shows the experimental results and gives the corresponding discussions. Finally, the conclusions are drawn in Section IV.

II. THz Photonic-Wireless Link

A. Experimental Setup

Figure 1 shows the experimental configuration of a high-speed single channel THz photonic-wireless transmission

system, including the spectra after the OFC generation and before the UTC-PD, as well as the DSP routine structure at the receiver. First, a continuous wave (CW) light from an external cavity laser (ECL, <100 kHz linewidth) at a wavelength of around 1550 nm is launched into two cascaded phase modulators (PMs), with a tunable optical delay line (ODL) in-between, to generate a coherent OFC. Both PMs are driven by a 25 GHz radio frequency (RF) sinusoidal signal, which determines the comb line spacing of the OFC. The amplified RF driving power on the two PMs (Vπ of 3V) are 31 dBm and 22 dBm, corresponding to the modulation indices of around 3.8Vπ and 1.4Vπ, respectively. The delay of the ODL in-between can be optimized to achieve a timing match between the two PMs, to broaden the optical spectrum for generating the desired THz carrier frequency. After amplified by using an Erbium-doped fiber amplifier (EDFA), the OFC with 25 GHz line spacing is fed into a programmable wave shaper (WS, Finisar 4000S) to be selected, separated and equalized into two comb lines with 425 GHz spacing, as two different output ports. In one port, a single optical tone is selected to act as a remote local oscillator (LO) for photo-mixing for THz signal generation. The other tone at the output of the other port, positioned at 425 GHz from the LO tone, is selected as a signal carrier and launched into an in-phase (I) and quadrature (Q) optical modulator (IQM) for data modulation. A two-channel arbitrary waveform generator (AWG, 64 GSa/s) is used to map and modulate two shifted pseudorandom binary sequence (PRBS) 2^{15}-1 sequences into a 16QAM signal at the IQM. The 16QAM signal waveform is pulse shaped with a root-raised-cosine (RRC) filter of 0.15 roll-off factor. Then a resampling process of the signal to match the AWG sampling rate of 64 GSa/s is performed. Static digital pre-equalization is performed prior to the modulation to pre-compensate the AWG output frequency roll-off and the skew between the two electrical cables. The optical carrier signal modulated with 16QAM after the IQM is amplified by an EDFA followed by an optical band-pass filter (OBPF) to remove out-of-band amplified spontaneous emission (ASE) noise. Here, a variable optical attenuator (VOA) is employed to control the power of the optical 16QAM signal before combining with the optical LO branch, to keep the power ratio balanced between the optical LO and signal, for the best photo-mixing efficiency in the UTC-PD. A polarization controller (PC) is placed in the optical 16QAM signal branch before a 3-dB coupler, to align the polarization states between the two branches. It should be noted that the two critical technical rules mentioned above are found to have significant impacts on the generated THz signal power and signal-to-noise ratio (SNR) with heterodyne mixing in the UTC-PD, thus requiring precise optimization [34]. After combining with the LO in the 3 dB coupler, the optical signal is amplified and filtered by an EDFA and OBPF respectively.

Finally, a polarizer pre-posed by a PC ensures the modulated optical tone and unmodulated LO are co-polarized to match the input polarization state of the UTC-PD. After that, a polarization maintaining (Pol. M) VOA is utilized to accurately control the incident optical power launched into the broadband UTC-PD for heterodyne mixing, while maintaining the matched polarization with the input of UTC-PD. The optical spectra of the generated OFC and the combined signals after the 3 dB coupler are shown in insets of Fig. 1. At the output of the broadband UTC-PD, a single channel THz 16QAM signal centered at around 425 GHz is generated by optical heterodyne mixing, and emitted into a 0.5 m free-space line-of-sight (LOS) link, where a pair of THz lenses with a 38 mm diameter and 50 mm focus length is employed to collimate the THz beam. At the wireless reception, the received single channel THz signal is down-converted at once to the intermediate frequency (IF) domain by using a sub-harmonic Schottky mixer operating at the 300-500 GHz band, driven by a 12-time frequency multiplied electrical LO. The electrical LO signal is tunable in the frequency range of 33.8-34.3 GHz, resulting in a corresponding IF carrier frequency ranging 13-19 GHz in accordance with the baud rate of transmitted signal. The IF output signal is amplified by a RF amplifier with around 21 dB gain and 40 GHz bandwidth, and then fed into a broadband real-time digital sampling oscilloscope (Keysight DSOZ634A Infiniium) with 160 GSa/s sampling rate and 63 GHz analog bandwidth, for analog-to-digital conversion, demodulation and communication performance analysis. The digital signals are processed and analyzed offline with a specifically designed DSP routine in a quasi-real-time manner with a loop probing the captured samples every ~6 seconds.

B. Digital Signal Processing (DSP) Routine

The structure of the DSP routine at the receiver is shown in Fig. 1 inset. In fact, the overall DSP routine utilized in this high-speed single channel THz photonic-wireless transmission experiment consists of a transmitter (Tx) DSP for pre-processing the signal before loading it to the AWG, and a receiver (Rx) DSP segment to perform post-processing for signal reconstruction and demodulation. Both Tx and Rx DSP algorithms are performed offline with MATLAB. The Tx DSP for pre-processing has been roughly described in part A of this Section, and the details of Rx DSP for post-processing will be introduced in the following of this part.

At the receiver, a 2-tap static post-emphasis filter is employed to compensate the limitation of receiver bandwidth. It should be noted that this process needs to be performed prior to the frequency down-conversion, because the low-pass filtering effect from the mixer to the IF signal is not symmetrical around the IF carrier but around DC, as shown in Fig. 2. Therefore, if the post-emphasis filtering is performed after frequency down-conversion and low-pass filtering, the baseband signal will have a low-pass asymmetry property, making it difficult to be further equalized. This is in line with the generic equalization concept that the last filtering effect occurred in the channel should be equalized first. The post-emphasis equalizer coefficients are optimized by observing the final bit-error-rate (BER) performance instead of observing the evenness of the signal spectrum, as there is a trade-off relation between the compensated filtering effect and the high-frequency noise enhancement. A digital frequency down-conversion is performed after the post-emphasis filter.

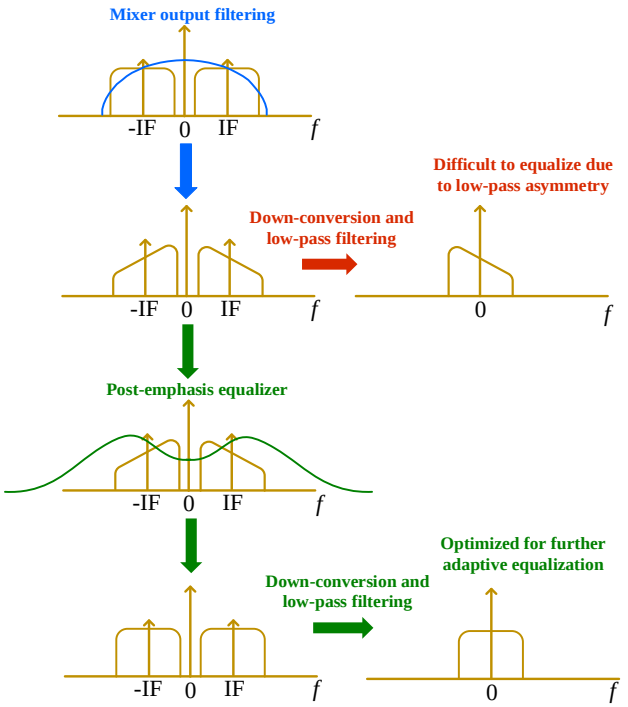

Fig. 2. Principle of the static post-emphasis equalization of the IF signal prior to frequency down-conversion to base band.

This process converts the real-valued IF signal into a complex baseband signal composing I and Q components, as illustrated in inset of Fig. 1. The detailed principle of this down-conversion process is derived in [34]. We have performed the clock recovery in a joint way that the complex baseband signal is firstly up-sampled to 8 samples per symbol. Then the sampling points within the symbol period that statistically provide maximum variance of amplitude are selected, indicating maximum eye diagram openings in both I and Q components are obtained.

In this work, an adaptive channel equalization is implemented based on a 29-tap lattice filter with the classical butterfly structure, which is driven by the multi-modulus algorithm (MMA) [35]. The algorithm performs blind equalization by minimizing the time-averaged mean-square error, and works independent of carrier frequency and phase which are still not available by this stage.

The frequency offset recovery (FOR) and phase noise compensation (PNC) are the essential blocks after the adaptive channel equalization to estimate and compensate for the phase noise introduced by the incoherent heterodyne beating between the optical signal and LO for frequency up-conversion. The schematic of the used 2-stage FOR and PNC scheme is described in Fig. 3. The first stage is based on QPSK partitioning and Viterbi & Viterbi (V&V) algorithm to recovery the frequency offset due to imperfect IF down-conversion [36]. First, the received symbols are sent into a decision circuit where the symbols are mapped into the closest amplitude radius in the 16-QAM constellation. Then, the angle between the mapped symbols and its closest QPSK angle is calculated and employed to angularly rotate the modulation component of the input symbols to QPSK positions. The normalized V&V algorithm utilizing the fourth power operation can now be used to remove the modulation and a block of $2M_1+1$ symbols is considered for additive white Gaussian noise (AWGN) mitigation. The calculated phase noise estimator needs to be unwrapped to reduce cycle slip occurrence, before being linearly fitted and differentiated to derive the estimated frequency offset. The estimated frequency offset at the output of the first stage is then applied to the transmitted signal, before feeding forward to the second stage for phase noise compensation based on blind phase search (BPS) [37]. A block of $2M_2+1$ symbols is rotated by a number of test phases, sent into a decision circuit module and the square distance to the closest constellation points is calculated. The test phase that provides the minimum distance error corresponds to the estimated phase rotation of the symbol block.

Finally, after the FOR and PNC block the symbols are decoded into binary format and the BER is counted by comparing the received binary sequence with the transmitted PRBS-15 sequence. It should be noted that the first two bits of the symbol is differentially Gray-decoded to determine the quadrant of the complex plane. This step is essential to eliminate burst errors induced by any cycle slips occurred during the FOR and PNC. The details of the differential decoding can be found in [37].

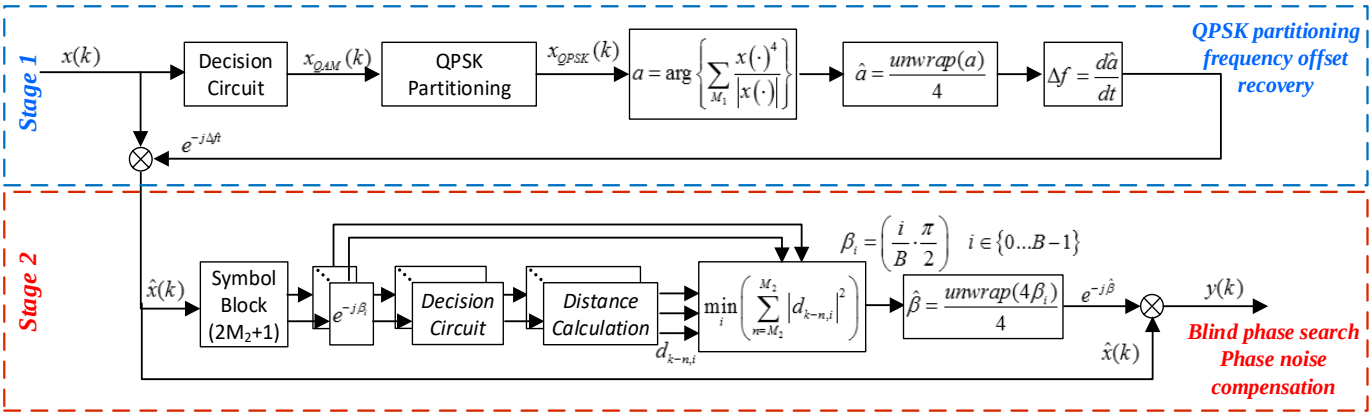

Fig. 3. Block diagram of the two-stage frequency offset recovery (FOR) and phase noise compensation (PNC) scheme used in this work. The first stage is frequency offset recovery based on QPSK partitioning method; the second stage if blind phase search (BPS) based phase noise compensation.

III. Results and Discussions

In this work, a single channel THz photonic-wireless transmission at the 0.4 THz band with 16QAM signal symbol rates of 16 Gbaud, 20 Gbaud, 28 Gbaud and 32 Gbaud have been investigated and experimentally evaluated, which correspond to line bit rates of 64 Gbit/s, 80 Gbit/s, 112 Gbit/s and 128 Gbit/s, respectively. As shown in Fig. 4(a), the BER performance for all cases of four different baud rates has been measured as a function of the incident optical power launched into the UTC-PD, and the below-FEC threshold performance in all cases are successfully achieved. It should be noted that both cases of 16 Gbaud and 20 Gbaud transmissions have realized the BER performance below the hard-decision forward error correction (HD-FEC) threshold of 3.8×10^{-3} with 7% overhead (7%-OH HD-FEC), reaching the error-free post-FEC net bit rates of 59 Gbit/s and 74 Gbit/s, respectively. In the cases of the 28 Gbaud and 32 Gbaud transmissions, the BER performances below the soft-decision FEC threshold of 2×10^{-2} with 20% overhead (20%-OH SD-FEC) are achieved, resulting in the overall post-FEC error-free net bit rates of 93 Gbit/s and 106 Gbit/s, respectively, as seen in Fig. 4(a). The corresponding signal constellations captured at 14 dBm for all the cases of four symbol rates are displayed in Fig. 4(b). We show the electrical spectra of the 32 Gbaud signal both before and after down conversion and filtering in Fig. 4(c). And the IF frequency for this baudrate is set to be 18.5 GHz. The overall performance of the wireless transmission system is basically limited by the SNR of the received signals and the IF bandwidth of the THz receiver. The former is primarily due to the low conversion efficiency of the UTC-PD (0.15 A/W) and the THz Schottky mixer (with around 17 dB conversion loss), and the latter further leads to the enhancement of the high frequency noise after post-emphasis equalization. The performance difference between different symbol rates can also be found from the spreading clusters of the corresponding 16QAM constellations. It should be noted that further increase of the incident optical power launched into the UTC-PD above 14 dBm cannot reach better BER performances, and this case can be attributed to the saturation of the UTC-PD in terms of THz output power. However, in the future, it is expected that a larger margin can be achieved by using multi-subcarrier modulation formats with higher noise tolerance, and THz emitters and receivers with enhanced performance. In addition, the THz power/low noise amplifiers and an optimized layout of THz lenses will be employed in the system to extend the wireless transmission distance for the future perspective.

Finally, the BER performance stability of the THz photonic-wireless communication system is evaluated in the lab environment, and the measured results are shown in Fig. 4(d). For each symbol rate, we run the system continuously over 25 minutes, collecting 250 traces with 800k samples per trace and counting errors. As seen in Fig. 4(d), it is observed that for all cases the system could maintain the BER performance within a small fluctuation range, below the corresponding FEC thresholds. This measurement indicates that the experimentally demonstrated THz photonic-wireless

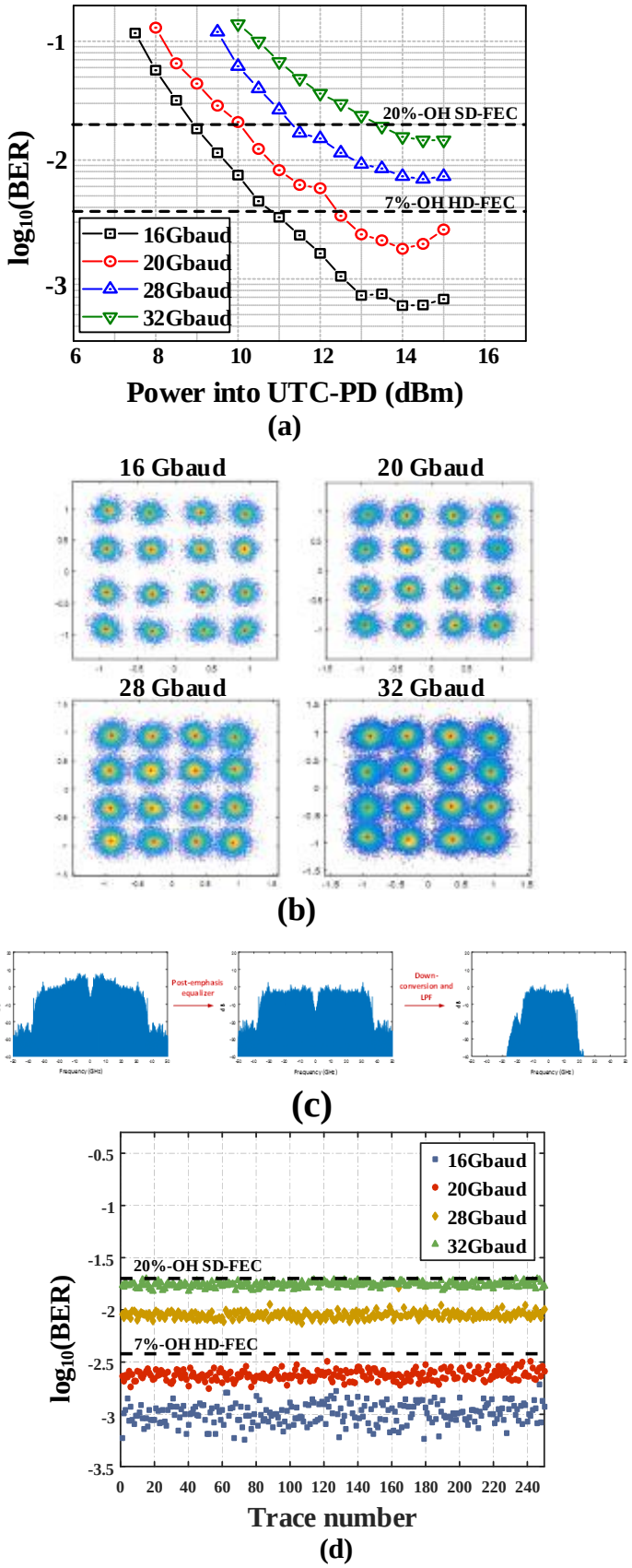

Fig. 4 (a). BER performance versus the incident optical power launched into the UTC-PD. (b). Constellations for all 4 baud rates at 14 dBm optical power. (c). The electrical spectra of the 32 Gbaud signal both before and after down conversion and filtering. (d). System stability tests for all 4 configurations (250 traces (~25 min) per channel, 800 k Sa/Trace).

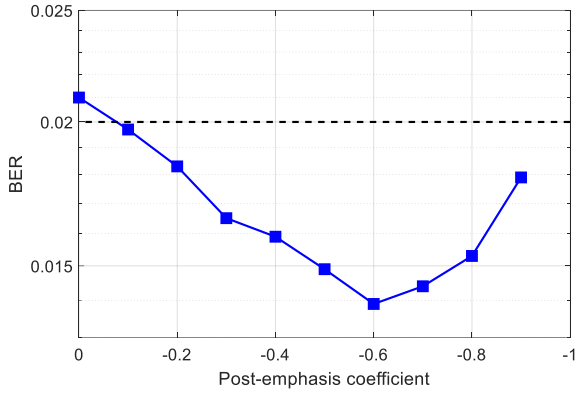

Fig. 5. The BER results of the 32 Gbaud signal at power into the UTC-PD of 15 dBm as a function of the post-emphasis coefficients.

link operating at high symbol rates is stable from system-wide implementation viewpoint because of the sophisticated DSP algorithms used in this work. In addition, in order to provide a clear picture of how the post equalization impacts on the demodulation performance, we sweep the 2nd tap coefficient of the 2-tap post filter from 0 (no post-emphasis) to -0.9 (strong post-emphasis). And the BER results of the 32 Gbaud signal at power into the UTC-PD of 15 dBm as a function of the post-emphasis coefficients are shown in Fig. 5.

IV. Conclusion

We have proposed and experimentally demonstrated a high-speed single channel THz photonic-wireless transmission system operating in the 0.4 THz band by using a single pair of THz emitter and receiver. The high throughput of up to 106 Gbit/s within a single channel in the THz band is enabled by employing spectrally efficient 16QAM modulation format, ultra-broadband THz transceivers and advanced DSP routine, without using any spatial MIMO, PDM or frequency division multiplexing techniques. The demonstration of high-speed THz wireless link beyond 100 Gbit/s shows stable transmission performance, indicating its high potential to support future UWNs and burgeon bandwidth-hungry ultrafast short-range wireless applications.

References

[1] S. Cherry, “Edholm’s law of bandwidth,” *IEEE Spectr.*, vol. 41, no. 7, pp. 58–60, Jul. 2004.

[2] “White paper: Cisco VNI Forecast and Methodology, 2015-2020.” [Online]. Available: http://www.cisco.com/c/en/us/solutions/collateral/service-provider/visual-networking-index-vni/complete-white-paper-c11-481360.html. Accessed: 2016.

[3] H. J. Song and T. Nagatsuma, “Present and future of terahertz communications,” *IEEE Trans. THz Sci. Technol.*, vol. 1, no. 1, pp. 256–263, Sep. 2011

[4] Y. Niu, Y. Li, D. Jin, L. Su, and A. V. Vasilakos, “A survey of millimeter wave communications (mmWave) for 5G: opportunities and challenges,” *Wirel. Netw.*, vol. 21, pp. 2657–2676, 2015.

[5] M. Tonouchi, “Cutting-edge terahertz technology,” *Nat. Photon.*, vol. 1, no. 2, pp. 97–105, Feb. 2007.

[6] G. Fettweis, F. Guderian, and S. Krone, in *Proc. IEEE Design, Automation & Test in Europe Conf. (DATE11)*, 2011, pp. 1–6.

[7] M. Pagani and H. Italia, “Microwave digital radio link transceivers: historical aspects and trends,” in *Proc. IEEE Int. Microwave Symp. (IMS2015)*, 2015, pp. Workshop WMH-2.

[8] T. Nagatsuma, G. Ducournau, and C. C. Renaud, "Advances in terahertz communications accelerated by photonics," *Nat. Photon.*, vol. 10, no. 6, pp. 371-379, Jun. 2016.

[9] A. J. Seeds, H. Shams, M. J. Fice, and C. C. Renaud, “Terahertz photonics for wireless communications,” *J. Lightw. Technol.*, vol. 33, no. 3, pp. 579–587, Feb. 2015.

[10] T. Kürner and S. Priebe, “Towards THz communications — status in research, standardization and regulation,” *J. Infrared Milli. Terahz Waves*, vol. 35, no. 1, pp. 53–62, Jan. 2014.

[11] X. Pang, A. Caballero, A. Dogadaev, V. Arlunno, R. Borkowski, J. S. Pedersen, L. Deng, F. Karinou, F. Roubeau, D. Zibar, X. Yu, and I. T. Monroy, “100 Gbit/s hybrid optical fiber-wireless link in the W-band (75–110 GHz),” *Opt. Exp.*, vol. 19, no. 25, pp. 24944–24949, Nov. 2011.

[12] X. Li, J. Yu, J. Zhang, Z. Dong, F. Li, and N. Chi, “A 400G optical wireless integration delivery system,” *Opt. Exp.*, vol. 21, no. 16, pp. 18812–18819, Aug. 2013.

[13] X. Li, Z. Dong, J. Yu, N. Chi, Y. Shao, and G. K. Chang, "Fiber-wireless transmission system of 108 Gb/s data over 80 km fiber and 2×2 multiple-input multiple-output wireless links at 100 GHz W-band frequency," Opt. Lett., vol. 37, no. 24, pp. 5106-5108, Dec. 2012.

[14] J. Yu, X. Li, J. Zhang, and J. Xiao, “432-Gb/s PDM-16QAM signal wireless delivery at W-band using optical and antenna polarization multiplexing,” in *Proc. Eur. Conf. Opt. Commun. (ECOC2014)*, Cannes, France, 2014, Paper We.3.6.6.

[15] X. Li, J. Yu, J. Xiao, Y. Xu, and L. Chen, "Photonics-aided over 100-Gbaud all-band (D-, W- and V-band) wireless delivery," in *Proc. 42nd Eur. Conf. Opt. Commun. (ECOC2016)*, Düsseldorf, Germany, Sep. 2016, Paper W.1.E.4.

[16] R. Puerta, J. Yu, X. Li, Y. Xu, J. Olmos, and I. Monroy, “Demonstration of 352 Gbit/s photonically-enabled D-band wireless delivery in one 2x2 MIMO system,” in *Proc. Opt. Fiber Commun. Conf. (OFC2017)*, Los Angeles, the USA, Mar. 2017, Paper Tu3B.3.

[17] S. Koenig, D. Lopez-Diaz, J. Antes, F. Boes, R. Henneberger, A. Leuther, A. Tessmann, R. Schmogrow, D. Hillerkuss, R. Palmer, T. Zwick, C. Koos, W. Freude, O. Ambacher, J. Leuthold, and I. Kallfass, “Wireless sub-THz communication system with high data rate,” *Nat. Photon.*, vol. 7, no. 12, pp. 977–981, Dec. 2013.

[18] H. Shams, T. Shao, M. J. Fice, P. M. Anandarajah, C. C. Renaud, F. V. Dijk, L. P. Barry, and A. J. Seeds, “100 Gb/s multicarrier THz wireless transmission system with high frequency stability based on a gain-switched laser comb source,” *IEEE Photon. J.*, vol. 7, no. 3, pp. 7902011, Jun. 2015.

[19] H. Shams, M. J. Fice, K. Balakier, C. C. Renaud, F. V. Dijk, and A. J. Seeds, “Photonic generation for multichannel THz wireless communication,” *Opt. Exp.*, vol. 22, no. 19, pp. 23465–23472, Sep. 2014.

[20] H. Shams, M. J. Fice, L. Gonzalez-Guerrero, C. C. Renaud, F. van Dijk, and A. J. Seeds, "Sub-THz Wireless Over Fiber for Frequency Band 220–280 GHz," *J. Lightw. Technol.*, vol. 34, no. 20, pp. 4786-4793, Oct. 2016.

[21] S. Koenig, F. Boes, D. Lopez-Diaz, J. Antes, R. Henneberger, R. Schmogrow, D. Hillerkuss, R. Palmer, T. Zwick, C. Koos, W. Freude, O. Ambacher, I. Kallfass, and J. Leuthold, "100 Gbit/s Wireless Link with mm-Wave Photonics," in *Proc. Opt. Fiber Commun. Conf. (OFC2013)*, Anaheim, California United States, the USA, 2013, Paper PDP5B.4.

[22] X. Yu, R. Asif, M. Piels, D. Zibar, M. Galili, T. Morioka, P. U. Jepsen, and L. K. Oxenløwe, “60 Gbit/s 400 GHz wireless transmission,” in *Proc. Int. Conf. Photon. Switching*, Florence, Italy, Sep. 2015, pp. 4–6.

[23] X. Yu, R. Asif, M. Piels, D. Zibar, M. Galili, T. Morioka, P. U. Jepsen, and L. K. Oxenløwe, "400-GHz Wireless Transmission of 60-Gb/s Nyquist-QPSK Signals Using UTC-PD and Heterodyne Mixer," *IEEE Trans. THz Sci. Technol.*, vol. 6, no. 6, pp. 765-770, Nov. 2016.

[24] S. Jia, X. Yu, H. Hu, J. Yu, T. Morioka, P. U. Jepsen, and L. K. Oxenløwe, "Experimental analysis of THz receiver performance in 80 Gbit/s communication system," in *Proc. 41st Int. Conf. Infrared Milli. THz Waves (IRMMW-THz 2016)*, Copenhagen, Denmark, Sep. 2016, pp. 1-2.

[25] S. Jia, X. Yu, H. Hu, J. Yu, T. Morioka, P. U. Jepsen, and L. K. Oxenløwe, “80 Gbit/s 16-QAM multicarrier THz wireless communication link in the 400 GHz band,” in *Proc. 42nd Eur. Conf. Opt. Commun. (ECOC2016)*, Düsseldorf, Germany, Sep. 2016, Paper W.1.E.5.

[26] S. Jia, X. Yu, H. Hu, J. Yu, T. Morioka, P. U. Jepsen, and L. K. Oxenløwe, “THz wireless transmission systems based on photonic generation of

highly pure beat-notes," *IEEE Photon. J.*, vol. 8, no. 5, pp. 7905808, Oct. 2016.

[27] S. Jia, X. Yu, H. Hu, J. Yu, P. Guan, F. D. Ros, M. Galili, T. Morioka, and L. K. OxenlØwe, "THz photonic wireless links with 16-QAM modulation in the 375-450 GHz band," *Opt. Exp.*, vol. 24, no. 21, pp. 23777-23783, Oct. 2016.

[28] S. Jia, X. Yu, H. Hu, J. Yu, T. Morioka, P. U. Jepsen, and L. K. Oxenløwe, "120 Gb/s multi-channel THz wireless transmission and THz receiver performance analysis," *IEEE Photon. Technol. Lett.*, vol. 29, no. 3, pp. 310-313, Feb. 2017.

[29] X. Yu, S. Jia, H. Hu, P. Guan, M. Galili, T. Morioka, P. U. Jepsen, L. K. Oxenløwe, "THz photonics-wireless transmission of 160 Gbit/s bitrate," in *Proc. 21st Optoelectron. Commun. Conf. Int. Conf. Photon. Switching (OECC & PS 2016)*, Niigata, Japan, Jul. 2016, Paper PD1-2.

[30] X. Yu, S. Jia, H. Hu, M. Galili, T. Morioka, P. U. Jepsen, and L. K. Oxenløwe, "160 Gbit/s photonics wireless transmission in the 300-500 GHz band," *APL Photon.*, vol. 1, no. 8, pp. 081301, Nov. 2016.

[31] X. Pang, S. Jia, O. Ozolins, X. Yu, H. Hu, L. Marcon, P. Guan, F. Da Ros, S. Popov, G. Jacobsen, M. Galili, T. Morioka, D. Zibar, L. K. Oxenløwe, "260 Gbit/s photonic-wireless link in the THz band," in *Proc. IEEE Photon. Conf., 29th Annual Conf. IEEE Photon. Society (IPC2016)*, Hawaii, the USA, Oct. 2016, Paper PD1-2.

[32] T. Ishibashi, Y. Muramoto, T. Yoshimatsu, and H. Ito, "Unitraveling-carrier photodiodes for terahertz applications," *IEEE J. Select. Topics in Quantum Electron.*, vol. 20, no. 6, pp. 79-88, Nov. 2014.

[33] X. Pang, S. Jia, O. Ozolins, X. Yu, H. Hu, L. Marcon, P. Guan, F. Da Ros, S. Popov, G. Jacobsen, M. Galili, T. Morioka, D. Zibar, L. K. Oxenløwe, "Single channel 106 Gbit/s 16QAM wireless transmission in the 0.4 THz band," in *Proc. Opt. Fiber Commun. Conf. (OFC2017)*, Los Angeles, the USA, Mar. 2017, Paper Tu3B.5.

[34] X. Pang, A. Caballero, A. Dogadaev, V. Arlunno, L. Deng, R. Borkowski, J. S. Pedersen, D. Zibar, X. Yu, and I. T. Monroy, "25 Gbit/s QPSK hybrid fiber-wireless transmission in the W-band (75–110 GHz) with remote antenna unit for in-building wireless networks," *IEEE Photon. J.*, vol. 4, no. 3, pp. 691-698, Jun. 2012.

[35] P. J. Winzer, A. H. Gnauck, C. R. Doerr, M. Magarini, and L. L. Buhl, "Spectrally efficient long-haul optical networking using 112-Gb/s polarization-multiplexed 16-QAM," *J. Lightw. Technol.*, vol. 28, no. 4, pp. 547-556, Feb. 2010.

[36] I. Fatadin and S. J. Savory, "Compensation of frequency offset for 16-QAM optical coherent systems using QPSK partitioning," *IEEE Photon. Technol. Lett.*, vol. 23, no. 17, pp. 1246-1248, Sep. 2011.

[37] T. Pfau, S. Hoffmann, and R. Noé, "Hardware-efficient coherent digital receiver concept with feedforward carrier recovery for M-QAM constellations," *J. Lightw. Technol.*, vol. 27, no. 8, pp. 989-999, Apr. 2009.